Liquid dispersion in packed columns: experiments and numerical modelling

Manel Fourati, Véronique Roig, Ludovic Raynal

Liquid dispersion in packed columns : experiments and numerical modeling.

M. Fourati[1,2], V. Roig[1] and L. Raynal[2*]

[1]IMFT, Université de Toulouse (INPT, UPS) & CNRS, Allée Camille Soula, 31400 Toulouse, France

[2]IFP Energies nouvelles, Rond-point de l'échangeur de Solaize BP3, 69360 Solaize, France

([*]Corresponding Author's E-mail: ludovic.raynal@ifpen.fr)

Abstract:

In order to optimize the design of gas-liquid packed columns used in distillation or in absorption processes, it is of high importance to be able to predict liquid dispersion. Indeed, dispersion phenomena will impact the choice and design of liquid distributing devices and the height of the packed beds. For this, one mainly relies on industrial feedback and on some experimental results obtained at laboratory scale which cannot be directly extrapolated since their geometric characteristics are at least one order of magnitude less than industrial columns in terms of columns diameter and height. To fill this gap CFD simulation tools should be more used since they can be used at any scale. However the latter option requires adequate modeling in particular for dispersion terms which are little studied due to the lack of data for validation. The present paper aims at developing, from original dispersion experimental measurements, closure laws that can be implemented in CFD codes. Liquid spreading from a source point has been investigated for the Mellapak 250.X via gamma-ray tomography measurements. Closure laws are discussed from a simple 1D model which enable to go further within the Eulerian two-fluid framework with original user-defined function and associated models that take into account liquid dispersion in the packed bed modeled as a porous medium with appropriate closure laws. The comparison between experiments and CFD results shows that the present approach is adequate and should be further developed in order to be more precise and adapted to more packings.

Keywords: CO_2 capture; distillation; packing; two-phase flow; liquid dispersion; CFD

1. Introduction

CO_2 Capture and Storage (CCS) is known to be a possible technology for carbon mitigation. IEA (IEA, 2009) considers that it could handle up to 19% of CO_2 emissions. Post-combustion capture using chemical solvents is one promising solution, especially when applied to coal-fired power plants, the largest industrial CO_2 emitters. However, the deployment of this technology requires process optimization with associated cost reduction, both in terms of operational expenditures (Opex) and capital expenditures (Capex). As underlined by Raynal *et al.* (2011), many studies are dedicated to new solvents identification, with the primary goal of reducing Opex, but less work deals with Capex reduction. The latter objective can be achieved by developing new high performance packings (Alix *et al.*, 2008 and 2011; Sulzer, 2011) and/or by achieving the most adequate design of packed columns. Such an optimum design is linked to the choice of packing, the number of packed beds and their height, the interaction between gas and liquid distributors with the gas/liquid flow within the packed bed. All these technical choices are strongly linked to liquid dispersion and gas/liquid interaction in the packed bed but it is today mostly given by industrial experience and little comes from more scientific explanations and deterministic calculations. To take all these phenomena into account for application to very large scale absorbers (CO_2 absorber are expected to be in the range of 8 to 14 m in diameter one order of magnitude above what can be done at laboratory scale), large scale two-fluid CFD simulations seem an appropriate tool. Some studies have started to focus on such aspects (Raynal and Royon-Lebeaud, 2007; Lappalainen *et al*, 2009), but they either do not take into account liquid dispersion or are restricted to catalytic beds which geometry significantly differs from modern packings. Present article deals with liquid dispersion in modern high efficiency metallic packings.

Recent experiments performed to characterize the dispersion of liquid in a counter-current gas-liquid packed column filled with structured or random packings are briefly reported and discussed in part 1. We then present the hydrodynamic model used to simulate the flow in the column (part 2). It is an Eulerian two-fluid model in which we include a specific model for liquid dispersion. The global model is discussed to analyze the physics associated to the various closure laws. We also discuss the

consistency of the model as well as the connection between experiments and modeling. In part 3 experimental results and numerical simulations are compared.

2. Experiments

In order to study the liquid dispersion, liquid distribution measurements have been performed with a high resolution tomographic system in a 400 mm diameter column of 1.5 m in height. The gas/liquid packed column is filled with Mellapak 250.X structured packing (geometric area per unit volume a_g=250 m^2/m^3, porosity ε=0.98 and angle of the flow channels with horizontal direction θ=60°). It is operated in the counter-current flow mode. Liquid is injected at top of the column in the central part of the column and counter-current gas flow is applied using a diffuser at the bottom of the column. A precise description of the experimental set-up is given in Fourati *et al.* (2012). Adapted liquid flow distributors have been used in order to generate the non-uniform liquid flow distribution at the top of the packed bed and tomographic liquid hold-up (also named liquid saturation θ_L) maps have been measured at different axial positions along the bed height. A sketch of the experimental set-up with the 4 axial positions, denoted z_i (i=1 to 4) at which tomography measurements have been performed, is given in Fourati *et a*l. (2012). The distances from the liquid inlet are z_1 = 32 cm, z_2 = 48 cm, z_3 = 74 cm and z_4 = 110.5 cm. Liquid hold-up measurements were carried out over a large range of experimental conditions: the liquid load being varied from 16 to 56m^3/m^2h and the gas kinetic factor from 20 to 80% of its flooding value. We also tested two couples of fluids: air-water or air-mono-ethanolamine with 30% mass fraction in water. Pressure drop measurements are also reported and discussed in Fourati *et al.* (2012).

In the present study we discuss air-water experiments and focus on low liquid load (q_L=16 m^3/m^2h) and gas kinetic factors F_S equal to 20% and 60% of the flooding condition F_C as determined from experiments (F_S=20%F_C=0.74 $Pa^{0.5}$ and F_S=60%F_C=2.21 $Pa^{0.5}$).

Figure 1 shows liquid retention maps obtained at the different axial positions along the bed for a liquid flow rate of q_L = 16 $m^3/m^2/h$ and a gas F-factor $F_S=\rho_G^{1/2}U_{GS}$ equal to 0.74 $Pa^{0.5}$ in case A and to

2.21 $Pa^{0.5}$ in case B. One observes that the liquid dispersion seems quite fast in the structured packing and that a homogeneous flow is almost achieved at position z_4 (1.1 m below liquid injection) whatever the gas flow rate. Positions z_1 and z_2 are located in the first packing element. This is the reason why, at these positions, liquid distribution remains aligned with the solid metal sheets of the packing for both cases. For downstream positions (z_3 and z_4), the liquid distribution is already isotropic. The liquid volume fraction still varies a lot at small scale, as liquid flows in films located along the solid matrix but the spreading of the liquid shows no significant heterogeneities at large scale. We can thus consider an homogeneous approach for modeling.

Liquid spread factors have also been determined from these maps in order to characterize liquid dispersion. The spread factor, D_r, is a length scale factor related to dispersion in a transport model for the liquid. We adopted an advection-diffusion transport equation for the liquid flow rate averaged at a meso-scale: q_L. In cylindrical coordinates, it is written as follows:

$$\frac{\partial q_L}{\partial z} = D_r \frac{1}{r}\frac{\partial}{\partial r}\left(r\frac{\partial q_L}{\partial r}\right)$$

The local liquid flow rate q_L is not measured directly. The liquid hold up being measured by tomography, we obtain q_L by using an experimental correlation obtained in homogeneous flows that gives $\theta_L = kq_L^{0.4}$ (Eq. (6) in Fourati *et al.*, 2012). Then, the comparison between the experimental results and a theoretical solution of $q_L(z,r)$, considering the spreading of liquid from a point source within an infinite packed-bed, gives access to the spread factor (Fourati *et al.*, 2012). We found that, changing the liquid and gas flow rates, the dispersion behavior remains identical whatever the flow conditions in the structured packing. For each run, we found a unique spread factor D_r=3.7 mm. We discuss in part 3 how such a dispersion coefficient D_r can be further used as a closure law in an Euler/Euler approach enabling accurate 3D simulations of complete columns.

3. Numerical model

We develop an Euler-Euler model solving local mass and momentum balances in gas and liquid phases to predict the hydrodynamics in packed columns. The transport equations deal with average

quantities that are volume-averaged over a representative elementary volume $\mathcal{V}$ with a length scale far smaller than the column size but large enough to give rise to well behaved averaged values.

The volume averaging procedure was well established by Whitaker and his collaborators in the framework of porous media (see as a starting point: Whitaker, 1973; Whitaker, 1986; and as a general reference: Whitaker, 1999). This averaging was also discussed by Liu (1999) and Liu and Masliyah (in Vafai, 2005) in order to prepare proposals for closure laws adapted to inertial two-phase flows in packings with high porosities. Several authors also discussed precisely the averaging for trickle-bed geometries taking into account or not partial wetting of the bed (Attou *et al.*, 1999; Iliuta and Larachi, 2005). Averaging for periodic packings and monoliths was also discussed by Mewes *et al.* (1999).

In the present study, we consider isothermal and incompressible flows, where both phases are Newtonian, with no mass transfer at the gas-liquid interface and no chemical reaction.

3.1. Primary equations

Geometric relations

The averaging procedure introduces the local volume fractions of each phases α_k, and their saturations θ_k. They are defined as $\alpha_k = \frac{\mathcal{V}_k}{\mathcal{V}}$ and $\theta_k = \frac{\mathcal{V}_k}{\mathcal{V}_G + \mathcal{V}_L}$ where $\mathcal{V}_k$ is the volume occupied by phase k (= G or L) and $\mathcal{V}$ includes the volume of solid. Both quantities are related by $\alpha_k = \varepsilon\theta_k$ through the porosity defined as $\varepsilon = \frac{\mathcal{V}_G + \mathcal{V}_L}{\mathcal{V}}$.

Due to the absence of overlapping of the phases, the geometric relation writes

$$\theta_G + \theta_L = 1 \tag{1}$$

Mass balances

In each phase the mass balance is written:

$$\frac{\partial}{\partial t}(\varepsilon\theta_k\rho_k) + \vec{\nabla}.(\varepsilon\theta_k\rho_k\vec{U}_k) = 0 \qquad \text{k=L, G} \tag{2}$$

where $\vec{U}_k$ is the intrinsic volume-average velocity of phase k defined as $\vec{U}_k = \frac{1}{\mathcal{V}_k}\int_{\mathcal{V}_k} \vec{u}_k dV$.

Momentum balances

In each phase the momentum balance is written, assuming that capillary effects are negligible for Mellapack packing due to large dimensions of the elementary channels:

$$\frac{\partial}{\partial t}(\varepsilon\theta_k\rho_k\vec{U}_k) + \vec{\nabla}.(\varepsilon\theta_k\rho_k\vec{U}_k.\vec{U}_k) = -\varepsilon\theta_k\vec{\nabla}P + \vec{\nabla}.(\varepsilon\overline{\overline{\tau_k}}) + \varepsilon\theta_k\rho_k\vec{g} + \varepsilon\vec{R}_{Ik} + \theta_k\vec{S}_{porous,k} + \vec{F}_{disp,k} \qquad \text{k=L, G} \quad (3)$$

We thus define a unique average pressure, denoted P, for both phases. The first term in the right hand side (r.h.s.) of Eq. (3) is the pressure force, the second term introduces the average stress tensor $\overline{\overline{\tau_k}}$. It is a viscous term that is often negligible because it involves spatial derivatives of the average velocity which are always far smaller than the spatial derivatives of the velocity at the scale of the elementary channel of the packing. The shear stresses and pressure forces acting in the representative elementary volume either at the interfaces or at the walls lead to the average momentum transfer terms $\varepsilon\vec{R}_{Ik}$ and $\theta_k\vec{S}_{porous,k}$ respectively. Their modeling is described in the following paragraph. The last term, denoted $\vec{F}_{disp,k}$, is a dispersive term that has been added to model forces leading to mechanical dispersion. Its origin and modeling is discussed further.

The interfacial momentum balance is then written neglecting capillary forces as:

$$\vec{R}_{IG} + \vec{R}_{IL} = \vec{0} \qquad (4)$$

The porosity that appears in mass and momentum balances is not a transported quantity. Its spatial distribution can be prescribed as resulting from the building of the packing. In the present work we choose a uniform porosity, ε=0.97.

3.2. Closure laws

Momentum transfers at the walls of the packing and at the gas-liquid interfaces

Recent proposals have been successfully tested to model the momentum transfers at the walls and at the gas-liquid interfaces in trickle-beds or structured packings (Holub *et al.*, 1993; Attou *et al.*, 1999; Iliuta *et al.*, 2004; Lappalainen *et al.*, 2008).

Momentum transfer at the walls

The proposed modellings for $\vec{S}_{porous,k}$ are issued from a generalized Ergun correlation primarily proposed for single-phase flows in packed beds (Ergun, 1952; Macdonald *et al.*, 1979):

$$\vec{S}_{porous,k} = -\left(\mu_k \overline{\overline{D}}_k \vec{U}_k + \frac{1}{2} \rho_k \left\| \vec{U}_k \right\| \overline{\overline{C}}_k \vec{U}_k \right) .$$

Reduced to its isotropic form this term writes:

$$\vec{S}_{porous,k} = -\left(\frac{\mu_k}{A_k} \vec{U}_k + \frac{1}{2} C_k \rho_k \left\| \vec{U}_k \right\| \vec{U}_k \right) \tag{5}$$

The resistance tensors $\overline{\overline{D}}_k$ and $\overline{\overline{C}}_k$ or their isotropic corresponding permeability A_k and coefficient C_k are modeled on a phenomenological basis to describe the effect, at a macroscale, of the complex geometry imposed by the solid matrix and of the flow regime at the microscale. The first term in Eq. (5) is dominant for viscous regimes, and the second one appears due to inertial effects. In single-phase flow (SP) and for the viscous regime, Kozeny-Carman scaling law extends Darcy law by giving the permeability A_k for complex or random porous geometries as a function of the averaged characteristic of the geometry. This law writes $A_{SP} = l^2 \varepsilon^2 / C_{CK}$ where l is an appropriate length scale usually taken equal to the inverse of the volumetric surface area a_ε^{-1} and C_{CK} is a constant generally equal to 5. This proposal gives reasonable permeabilities for random packings of spheres, periodic arrays of spheres or fractal porous media, but is not sufficient for multiscale geometries (Valdes-Parada *et al.*, 2009).

Ergun proposal for single-phase flows introduces inertial effects appearing as the second term in Eq. (5) also named Forchheimer correction. For non negligible velocities, the dependence of $\vec{S}_{porous,k}$ upon the square value of the velocity was theoretically demonstrated by Whitaker (1996) even if this was already well-known from experimental evidence. It is important to notice that this inertial effect is

additional to the viscous one, and that it does not replace it. In fact, inertial effects are not associated to a laminar-turbulent transition in the flow at the pore scale as they appear in infinite straight pipes. This is clear as they appear for Reynolds numbers in the pores smaller than 100. They must be understood as supplementary form drag linked to additional spatial accelerations at the pore scale appearing with flow recirculations for example (as discussed by Prieur du Plessis, 1994). Following Ergun first proposal the coefficient C_k is usually taken as proportional to $\frac{a_g}{6\varepsilon^2}$.

In two-phase flows, usually, to model each transfer term at the walls $\vec{S}_{porous,k}$, permeabilities have been adapted. The permeabilities are linked to an hydraulic diameter at the microscale of the involved phase. They are thus related to the porosity ε, the effective area a_g and the phase saturations θ_k (Holub *et al.*, 1993; Larachi *et al.*, 2004). Another difficulty due to two-phase flow is to take into account the wetting of the solid surface in the models. A fractional wetted area f_e is introduced to weight the momentum transfer terms. When $f_e = 1$, at locations where gas and liquid phases co-exist, the liquid is assumed to wet totally the walls and there is no shear stress at the walls for the gas. Of course, in single-phase regions occupied by gas alone, the momentum transfer at the wall of the porous medium is retained. In order to simulate partial wetting ($f_e < 1$), we have applied the general formulation of the model by Lappalainen *et al.* (2009): the momentum transfer at the walls and at the interfaces are respectively weighted by f_e, $(1-f_e)$ and f_e for the liquid, for the gas and for the gas-liquid interface (see Eq. (6) to (8) hereafter).

Iliuta et al. (2004) or Iliuta and Larachi (2005) have proposed closures specific for structured packing:

$$\vec{S}_{porous,L} = -f_e\left(\frac{E_1}{36}\times\frac{a_g^2 f_e}{\varepsilon\theta_L^2}\mu_L + \frac{E_2}{6}\frac{a_g}{\theta_L}\rho_L\left\|\vec{U}_L\right\|\right)\vec{U}_L = -K_{LS}\vec{U}_L \tag{6}$$

$$\vec{S}_{porous,G} = -(1-f_e)\left(\frac{E_1}{36}\times\frac{a_g^2}{\varepsilon}\mu_G + \frac{E_2}{6}a_g\rho_G\theta_G\left\|\vec{U}_G\right\|\right)\vec{U}_G = -K_{GS}\vec{U}_G \tag{7}$$

Both closure laws have similar mathematical forms with different length scales: $6a_g^{-1}$ for the gas phase and $\frac{\theta_L}{a_g}$ which is representative of the liquid film thickness. In the present work we have retained the

model of Iliuta and Larachi (2004) with their values of E_1 and E_2 (for Mellapak 250.X: $E_1 = 160$ and $E_2 = 0.16$). Strickly speaking, inside the parenthesis in Eq. (6) the wetting efficiency f_e is approximated equal to 1. We just keep the multiplying factor f_e in $\vec{S}_{porous,L}$ and resp. $(1-f_e)$ in $\vec{S}_{porous,G}$.

Momentum transfer at the gas-liquid interfaces

The general closure law adopted for the momentum transfer at the gas-liquid interfaces is similar to those at the walls. From Iliuta and Larachi (2004) we have:

$$\vec{R}_{IG} = -f_e\left(\frac{E_1}{36}\times\frac{a_g^2\theta_G}{\varepsilon^2(1-\frac{\theta_L}{f_e})^2}\mu_G + \frac{E_2}{6}\frac{a_g{\theta_G}^2}{\varepsilon(1-\frac{\theta_L}{f_e})^2}\rho_G\left\|\vec{U}_G-\vec{U}_L+\frac{\theta_L}{\theta_G}(1-\frac{1}{f_e})\vec{U}_L\right\|\right)\left(\vec{U}_G-\vec{U}_L+\frac{\theta_L}{\theta_G}(1-\frac{1}{f_e})\vec{U}_L\right)$$

For Mellapak 250.X and in normal operating conditions the order of magnitude of f_e is 1 and $\vec{U}_G-\vec{U}_L >> \frac{\theta_L}{\theta_G}(1-\frac{1}{f_e})\vec{U}$. We thus adopt the simplified model:

$$\vec{R}_{IG} = -f_e\left(\frac{E_1}{36}\times\frac{a_g^2}{\varepsilon^2\theta_G}\mu_G + \frac{E_2}{6}\frac{a_g}{\varepsilon}\rho_G\left\|\vec{U}_G-\vec{U}_L\right\|\right)\left(\vec{U}_G-\vec{U}_L\right) = -K_{IG}\left(\vec{U}_G-\vec{U}_L\right) \quad (8)$$

Discussion

To our knowledge there are no theoretical derivations of permeability expressions in two-phase flows except for a set of parallel non-connected identical tubes in pure viscous laminar regime (Bacri *et al.*, 1990). The present model (Eq. (6)-(8)) is based on the idea that Ergun general correlation can be used to reproduce the momentum transfers at the walls or at the interfaces, provided pertinent velocity and permeability are chosen for each transfer term. The values of the factors E_2 and E_2 are also taken unchanged in $\vec{S}_{porous,L}$, $\vec{S}_{porous,G}$ and $\vec{R}_{IG}$. We would like to show, with a simple example, that such proposal is of course of great interest in the absence of theoretical one, but that it has to be taken with care.

Holub *et al.* (1993) and then Iliuta *et al.* (2000) developed semi-analytical models where the porous medium is divided in slits in which the two-phase film flow is modeled before applying slit to bed relations to obtain macroscopic models of $\vec{S}_{porous,k}$ and $\vec{R}_{IG}$. Holub *et al.* (1993) developed a slit model for liquid films totally wetting the solid, while Iliuta *et al.* (2000) developed a double-slit method to take into account partial wetting. We retain their idea to analyze an ideal porous medium consisting in a set of parallel non-connected identical slits, but we follow, similarly to Bacri *et al.* (1990) an analytical approach based on Navier-Stokes resolution for steady, developed, laminar incompressible flow at the scale of the slit. This reduces the generality of the expected model but allows discussing the origin of the closed terms.

Let us consider first the analytical solution of the flow between two fluids (subscripts 1 and 2) confined in a plane channel of width h flowing along direction x (co-currently or with a countercurrent configuration). Due to gravity or to inertia in the vertical case, phases are assumed to be separated so that the flow is associated to a wetting efficiency equal to ½. The averaged values of the velocities and of the widths of both phases are denoted U_1, U_2, h_1 and h_2. The signs of U_1 and U_2 define co-current or counter-current flows. We can solve the Navier-Stokes equations in each phase which are coupled by the boundary condition at the fluid interface. The velocity components in (x, y) plane are denoted (u_k, v_k). Assuming a parallel flow, the continuity equations write:

$$v_k(y) = 0 \qquad \text{(k=1, 2)} \qquad \text{(D1)}$$

Momentum balances reduce to:

$$\mu_k \frac{du_k}{dy} = K_k \quad \text{where} \quad K_k = \frac{dP_k}{dx} - \rho_k g \sin(\theta) \qquad \text{(k=1, 2)} \qquad \text{(D2)}$$

with the following boundary conditions (BC) :

(BC1) $u_1 = 0$ at y=0

(BC2) $u_1 = U_I$ at y=h_1

(BC3) $u_2 = 0$ at y=h=h_1+h_2

(BC4) $u_2 = U_I$ at y=h_1

where h_1 and U_I the position and velocity of the interface are unknown.

The velocity profiles $u_k(y)$ can then be obtained and expressed using K_k, U_I, h and h_1. By integrating these velocity profiles in the y direction, one can relate the average velocity of each fluid to the interface velocity and pressure gradient:

$$U_k = \frac{U_I}{2} - \frac{K_k h_k^2}{12\mu_k} \qquad \text{(k=1, 2)} \qquad \text{(D3)}$$

The shear stresses at the walls and on each side of the interface can also be expressed as:

$$\tau_{w1} = -\mu_1 \frac{dU_1}{dy}\bigg)_{y=0} = -\mu_1\left(\frac{U_I}{h_1} - \frac{K_1 h_1}{2\mu_1}\right) = -\frac{\mu_1}{h_1}\left(6U_1 - 2U_I\right) \qquad \text{(D4)}$$

$$\tau_{w2} = \mu_2 \frac{dU_2}{dy}\bigg)_{y=h} = \frac{\mu_2}{h_2}\left(2U_I - 6U_2\right) \qquad \text{(D5)}$$

$$\tau_{I1} = \mu_1 \frac{dU_1}{dy}\bigg)_{y=h_1} = \mu_1\left(\frac{U_I}{h_1} + \frac{K_1 h_1}{2\mu_1}\right) = \frac{\mu_1}{h_1}\left(4U_I - 6U_1\right) \qquad \text{(D6)}$$

$$\tau_{I2} = -\mu_2 \frac{dU_2}{dy}\bigg)_{y=h_1} = \frac{\mu_2}{h_2}\left(4U_I - 6U_2\right) \qquad \text{(D7)}$$

The last boundary condition that must be verified is the continuity of the shear stress at the interface ((BC5) $\tau_{I1} + \tau_{I2} = 0$). This leads to:

$$U_I = \frac{3}{2}\left(\frac{\frac{\mu_1}{h_1}U_1 + \frac{\mu_2}{h_2}U_2}{\frac{\mu_1}{h_1} + \frac{\mu_2}{h_2}}\right) \qquad \text{(D8)}$$

The prediction of the position of the interface h_1 for the fully developed flow could be achieved by equating the pressure gradients in each fluid. For our present purpose we just rewrite the shear stresses using the known value of U_I:

$$\tau_{I2} = 6\frac{(U_1 - U_2)}{\frac{h_1}{\mu_1} + \frac{h_2}{\mu_2}} \qquad \text{(D9)}$$

$$\tau_{w1} = -3\frac{\mu_1}{h_1}U_1 - 3\frac{(U_1 - U_2)}{\frac{h_1}{\mu_1} + \frac{h_2}{\mu_2}} \qquad \text{(D10)}$$

$$\tau_{w2} = -3\frac{\mu_2}{h_2}U_2 + 3\frac{(U_1 - U_2)}{\frac{h_1}{\mu_1} + \frac{h_2}{\mu_2}} \qquad \text{(D11)}$$

We must notice that, if the velocity that appears in the interfacial shear stress is the relative velocity between both phases, the general expression for the shear stress of phase k at the wall is not simply related to the average velocity of phase k. The relative velocity also appears in τ_{w1} and τ_{w2}.

At the slit scale the momentum equations then write:

$$0 = -\theta_{ks}\frac{dP}{dx} + \theta_{ks}\rho_k g\sin(\theta) + F_{Ik} + F_{wk} \qquad \text{(k=1, 2)} \qquad \text{(D12)}$$

with $\theta_{ks} = \frac{h_k}{h}$ the volume fraction at the slit scale, and $F_{Ik} = \frac{\tau_{Ik}}{h}$, $F_{w1} = \frac{\tau_{w1}}{h}$.

We now apply an elementary homogenization method to obtain the macroscopic equations valid for the porous medium from the local solution in a slit. We consider that the porous geometry consists in an array of parallel slits. The variables describing the slit geometry are related by slit-to-bed relations to the macroscopic properties of the porous medium. These relations express that volume fraction of each phase and of the solid, as well as the intrinsic velocity or pressure averages are the same at the macroscopic scale and in the representative slit. We can thus write in a volume-average sense:

$$0 = -\varepsilon\theta_{ks}\frac{dP}{dx} + \varepsilon\theta_{ks}\rho_k g\sin(\theta) + \varepsilon F_{Ik} + \varepsilon F_{wk} \qquad \text{(k=1, 2)} \qquad \text{(D13)}$$

For a homogeneous flow, a comparison with Eq. (3) leads to the following relation where we used the analytical solution to express the shear stress terms:

$$\varepsilon R_{Ikx} + \theta_k S_{porous,kx} = +\varepsilon F_{Ik} + \varepsilon F_{wk} = \frac{6\varepsilon}{h^2}(-1)^k\frac{(U_1 - U_2)}{\frac{\alpha_1}{\mu_1} + \frac{\alpha_2}{\mu_2}} - 3\varepsilon\frac{\mu_k}{h^2\alpha_k}U_k + \frac{3\varepsilon}{h^2}(-1)^k\frac{(U_1 - U_2)}{\frac{\alpha_1}{\mu_1} + \frac{\alpha_2}{\mu_2}} \qquad \text{(D14)}$$

It must be recalled that the first term on the r.h.s. is due to interfacial shear stress and that the second and third terms are due to shear at the wall. Therefore semi-empirical models based on the idea that wall and interfacial momentum transfers are naturally linear relative to the phase velocity and respectively to the gas-liquid slip velocity ($\vec{S}_{porous,k} = -K_{kS}\vec{U}_k$ and $\vec{R}_{IG} \approx K_{IG}(\vec{U}_G - \vec{U}_L)$) have a limited theoretical basis and can be misleading. It is important to understand that the cutting between the momentum transfer terms at the walls and at the interface is not so obvious.

In the proposed modeling, we have to go further and interpret $\vec{S}_{porous,k}$ and $\vec{R}_{IG}$ no longer as wall and interfacial momentum transfer terms, but instead, as the closure laws respectively proportional to $\vec{U}_k$ and to $(\vec{U}_G - \vec{U}_L)$. We can rewrite the previous relation using Eq. (6)-(8):

$$\varepsilon K_{Ik}(U_1 - U_2) + \theta_k K_{ks} U_k = \frac{6\varepsilon}{h^2}(-1)^k \frac{(U_1 - U_2)}{\frac{\alpha_1}{\mu_1} + \frac{\alpha_2}{\mu_2}} - 3\varepsilon \frac{\mu_k}{h^2 \alpha_k} U_k + \frac{3\varepsilon}{h^2}(-1)^k \frac{(U_1 - U_2)}{\frac{\alpha_1}{\mu_1} + \frac{\alpha_2}{\mu_2}} \quad \text{(D15)}$$

By identification, the analytical solution of the laminar two-phase channel flow leads then to the following coefficients:

$$K_{Ik} = \frac{9}{\varepsilon h^2}(-1)^k \frac{1}{\frac{\theta_1}{\mu_1} + \frac{\theta_2}{\mu_2}} \quad \text{(D16)}$$

$$K_{ks} = 3\frac{\mu_k}{h^2 \theta_k^{\,2}} \quad \text{(D17)}$$

We now compare this result obtained from theoretical considerations, to the viscous parts of the models proposed in Eq. (6) to (8).

For the ideal porous medium consisting in parallel slits the relation $a_g = \frac{2\varepsilon}{h}$ applies. The viscous contribution in Eq. (6) and (7) therefore can be written:

$$K_{Ls} = 4\varepsilon f_e^{\,2} \frac{E_1}{36} \frac{\mu_L}{h^2 \theta_L^{\,2}} \quad \text{and} \quad K_{GS} = 4\varepsilon(1 - f_e) \frac{E_1}{36} \theta_G^{\,2} \frac{\mu_G}{h^2 \theta_G^{\,2}}$$

For partial wetting ($f_e = 0.5$), for porosity and gas volume fraction around 1, these relations lead to $K_{Ls} \approx 4.4 \frac{\mu_L}{h^2 \theta_L^{\,2}}$ and $K_{GS} \approx 8.8 \frac{\mu_G}{h^2 \theta_G^{\,2}}$. The orders of magnitude of the multiplicative factors are therefore in agreement with that found in Eq. (D17) but differences still remain. It must be noticed that the scalings with ε and θ_G are different. For Mellapak 250.X this is not so important because ε and θ_G are both around unity, but revising the scalings could be interesting for other packings.

The coefficient for the viscous contribution to the interfacial momentum transfer (Eq. (8)) also writes for our ideal porous medium:

$$K_{IG} = 4f_e \frac{E_1}{36} \frac{1}{h^2 \theta_G} \mu_G = 4f_e \frac{E_1}{36} \varepsilon \frac{1}{\varepsilon h^2 \frac{\theta_G}{\mu_G}} \approx \frac{8.8}{\varepsilon h^2 \frac{\theta_G}{\mu_G}} \quad \text{(D18)}$$

which is similar to (D16) for gas-liquid systems when $\frac{\theta_G}{\mu_G} >> \frac{\theta_L}{\mu_L}$ which is verified for our flow configurations.

As a conclusion on the discussion about momentum transfer modeling we can say that theoretical models in elementary configurations as proposed here can help discussing the validity of efficient semi-empirical models as proposed in Eq. (6) to (8) which have been widely tested and prove to be predictive. The discussion about the viscous parts of the closure laws shows that subject to model simultaneously wall and interfacial transfer terms, their global effect is correctly taken into account, even if semi-empirical models report walls effects in $\vec{R}_{IG}$, thus distorting the physical meaning of $\vec{S}_{porous,k}$ and $\vec{R}_{IG}$ terms.

Dispersion term

In two-phase flows through porous media, dispersion terms appear due to volume averaging in the equations of momentum. Two distinct elementary mechanisms lead to momentum dispersion. The first one is the difference of pressures across the fluid interface due to capillarity: it leads to the macroscopic effect called *capillary dispersion*. The second one is the complex advection of momentum by the fluid at the pore scale. Local velocities of the phases are in general different from the volume-averaged velocities, and for inertial flows, when these deviations are correlated at the macroscopic scale, this leads to *mechanical dispersion*. In fact, the volume averaging of the non linear terms in the local momentum equation introduces in the macroscopic equation the divergence of the velocity correlation tensor (Whitaker, 1973) which can be understood as an analogous to the Reynolds stress tensor in turbulence (Grosser *et al.*, 1988).

Capillary dispersion models

To take into account capillary dispersion, the first way could be to keep two pressures (one for each phase) in the macroscopic equations (Whitaker, 1986). But most often two-fluid eulerian models use a unique pressure identified as the pressure in the gas phase and introduce a closure law for the capillary pressure $P_c = P_G - P_L$. In such approach Eq. (3) for the liquid phase should include a dispersion term $\vec{F}_{disp,L,c} = \varepsilon P_c \vec{\nabla} \theta_L$ such as proposed by Attou and Ferschneider (2000), Boyer *et al.* (2005) or Jiang *et al.* (2002). The capillary pressure, which is related to interface curvature through Laplace law, is then given as a function of the liquid volume fraction at the macro-scale (Attou and Ferschneider, 2000; Boyer *et al.*, 2005). For general porous media or for trickle-beds the closure law for $P_c(\theta_L)$ is either obtained from experimental tests leading to a correlation introducing the Leverett function, or obtained from geometrical considerations about the gas-liquid interface curvature at the pore scale (Attou and Ferschneider, 2000; Jiang *et al.*, 2002; Lappalainen *et al.*, 2009-b). Lappalainen *et al.* (2009) used a different model for capillary dispersion. They wrote in the momentum equation of the liquid phase: $\vec{F}_{disp,L,c} = \varepsilon \theta_L \vec{\nabla} P_c$ which is not equivalent to the aforementioned term. Careful discussion of the modeling of this capillary dispersion term would be required to see the validity of such proposal.

In our study of structured packings, we do not take into account the capillary dispersion. This approximation is justified because the size of the packing elements is quite large so that we can argue that capillary pressure vanishes. Even if the curvature of the interface varies a lot at the pore scale we can give arguments that lead to neglect capillary pressure in our study. It is interesting to notice from Whitaker (1986) (eq. 3.14) that volume-averaged pressures of each phases P_L and P_G are not simply related to the volume-averaged value H of the interface curvature. The complete momentum interfacial relation includes normal viscous forces. The relation between the orders of magnitude then writes:

$$P_G - P_L = 2\sigma H + o\left(\max_k \left(\frac{\mu_k \left| \vec{U}_k \right|}{l_k} \right) \right)$$

where l_k is the size of phase k at the pore scale. In our flow conditions the second term on the r.h.s. is due to the liquid phase. Estimating l_k as the liquid film width e, and e as $\frac{\theta_L}{a_g}$, we find that this second term is around 0.5 Pa which is negligible. Taking the averaged value of H equal to the inverse of the hydraulic diameter ($\frac{4\varepsilon}{a_g}$), we also find that $2\sigma H$ is negligible since it is about 6 Pa, keeping in mind that viscous effects are of the order of 10^5 Pa. The capillary pressure can thus be neglected.

Mechanical dispersion

Most theoretical analysis of flows in porous media are applied to single-phase flows in saturated viscous regimes with linear momentum equation at the pore scale so that there is no momentum dispersion. In such case, dispersion only appears in volume-averaged equations for the scalar transport due to the presence of advection and to specific surface integrals at the boundaries of the phase (Quintard and Whitaker, 1993). This may be the reason why existing models about dispersion in porous media have been mainly developed for scalar transport (Brenner, 1980; Carbonell and Whitaker, 1983; Eidsath *et al.*, 1983; Liu and Masliyah in Vafai, 2005).

In two-phase flows through packings, inertia, interphase interactions and solid-phase interactions must be retained in volume averaged equations. In order to build such a system of volume averaged equations also able to reproduce dispersion, Liu (1999) proposed a volume-averaged approach including tortuosity effect and specific volume averaging rules. This approach introduces unclosed dispersion terms in mass and momentum equations. Liu and Long (2000) discussed a simplified version of the model for which they proposed semi-empirical closure laws. The assumptions of isotropic porous medium and of total wetting were introduced, but the generality of their proposal is unclear. It consists in adding in the momentum equation of the liquid phase a dispersive force $\vec{F}_{disp,L,1} = \vec{\nabla}.\left(\varepsilon\rho_L \overline{\overline{K}}_L.\vec{\nabla}(\frac{\theta_L \vec{U}_L}{\tau_L}) \right)$ originating from the interaction of the liquid and the solid matrix, and in each momentum equation another dispersive force originating from interactions of both phases which

writes for the gas phase $\vec{F}_{disp,IG} = \vec{\nabla}.\left(\varepsilon \rho_G \overline{\overline{K}}_{IG^*}.\vec{\nabla}(\frac{\vec{U}_G}{\tau_G} - \frac{\theta_L \vec{U}_L}{\tau_L \theta_L}) \right)$ and $-\vec{F}_{disp,IG}$ for the liquid. In these models τ_k are the tortuosities of the phases, $\overline{\overline{K}}_L$ and $\overline{\overline{K}}_{IG^*}$ the dispersion tensors modeled from the analysis of passive scalar dispersion results.

One can find in the chemical engineering literature several other semi-empirical proposals to model the mechanical dispersion forcing terms $\vec{F}_{disp,k}$ governing liquid spreading. But these models are scarcely described and have most often no definitive theoretical basis except that their form is adequate to introduce dispersion. Moreover, to our knowledge, the only closure to have been tested with a comparison between numerical simulations and experimental results is the one of Lappalainen et al. (2009, 2011). Mewes *et al.* (1999) introduced a general form able to generate an anisotropic dispersion term in the momentum equation of the liquid phase. It would write in our system of notations: $\vec{F}_{disp,L} = \overline{\overline{\xi}}.\left(\overline{\overline{S}}.(\varepsilon \theta_L \vec{U}_L)\right)$ where $\overline{\overline{\xi}}$ is a resistance tensor associated to shear stress at the walls that takes the simplified form $\overline{\overline{\xi}} = -\frac{K_{LS}}{\varepsilon}\overline{\overline{I}}_d$ for our isotropic model, and $\overline{\overline{S}}$ is a spreading tensor for which no closure law is proposed by the authors.

The discrepancy between the general models for mechanical dispersion proposed by Liu and Long (1999), Mewes *et al.* (1999) and Lappalainen *et al* (2009, 2011) shows that fundamental work is required to deduce dispersion terms from volume averaging of local balances. In the present work, we have retained the model tested by Lappalainen *et al.* (2009, 2011). It consists in adding in the momentum equations of both phases the following terms:

$$\vec{F}_{disp,L} = \theta_L K_{LS} \vec{U}_{D,L} - \varepsilon K_{IG}(\vec{U}_{D,G} - \vec{U}_{D,L}) \tag{9}$$

$$\vec{F}_{disp,G} = \theta_G K_{GS} \vec{U}_{D,G} + \varepsilon K_{IG}(\vec{U}_{D,G} - \vec{U}_{D,L}) \tag{10}$$

where $\vec{U}_{D,G} = -\frac{S\|\vec{U'}_G\|}{\alpha_G}\vec{\nabla}\alpha_G$ and $\vec{U}_{D,L} = -\frac{S\|\vec{U}_L\|}{\alpha_L}\vec{\nabla}\alpha_L$ are drift velocities and $\vec{U'}_G = \frac{\vec{U}_G}{\alpha_G}$, S is a spread factor whose dimension is length. Lappalainen *et al.* identified the present spread factor with the one obtained from liquid flow rate distributions interpreted with a convection-diffusion equation of q_L as

written in part 2 of the present paper. We discuss briefly hereafter the physics underlying the validity of such assumption. The proposal of Lappalainen *et al.* also assumes isotropic dispersion, and dispersion driving terms for both liquid and gas. In our flow regime, with high porosity and very thin liquid films, an order of magnitude study shows that the most important term ensuring liquid dispersion is $\vec{F}_{disp,L} = \theta_L K_{LS} \vec{U}_{D,L}$ which was indeed verified with numerical tests.

Discussion

It is important to notice that a spreading coefficient appears in this model. It is possible to identify this spreading coefficient with the spreading factor measured from the experiments assuming a convection-diffusion transport equation for the mass flow rate of the liquid as we did in part 2. This can be done if we assume that the dominant terms in the horizontal momentum balance for the liquid phase are related to shear stress at the walls and to dispersive term:

$$\left(\theta_k \vec{S}_{porous,L} + \vec{F}_{disp,L}\right)\vec{e}_h = 0 \tag{11}$$

where $\vec{e}_h$ is the horizontal unit vector. In cylindrical coordinates, with $\vec{e}_h = \vec{e}_r$, the balance then writes:

$$-K_{LS}\theta_L U_{Lr} - K_{LS} S \left\|\vec{U}_L\right\| \frac{\partial \theta_L}{\partial r} = 0 \quad \text{that is} \quad \theta_L U_{Lr} = -S \left\|\vec{U}_L\right\| \frac{\partial \theta_L}{\partial r}$$

This is equivalent to neglect accelerations, pressure gradients and gas-liquid interactions in the horizontal direction. This equilibrium leads to identify the horizontal average and drift liquid velocities in the mass balance of the liquid. For steady state flow, it writes:

$$\frac{\partial \theta_L U_{Lz}}{\partial z} + \frac{1}{r}\frac{\partial}{\partial r}\left(-rS\left\|\vec{U}_L\right\| \frac{\partial \theta_L}{\partial r}\right) = 0$$

From the mass balance in the liquid phase, assuming that $U_{Lz} \approx \left\|\vec{U}_L\right\|$ is nearly uniform, one can thus obtain the modeled convection-diffusion transport equation for the liquid flow rate $q_L = \theta_L U_{Lz}$:

$$\frac{\partial \theta_L U_{Lz}}{\partial z} \approx S \frac{1}{r}\frac{\partial}{\partial r}\left(r \frac{\partial \theta_L U_{Lz}}{\partial r}\right)$$

Under the assumption of the previous peculiar momentum equilibrium, it is therefore possible to identify the spread factor determined from our global analysis of the experimental distribution of liquid flow rate (D_r) with the spread factor of the model (S) used by Lappalainen *et al.* (2009).

Fractional wetting area

For structured packings, the effective specific area of the solid may be lower than the geometric one which indicates partial wetting. Several studies found in literature focused on the ratio between effective surface area (equivalent here to wetted area) and the geometric one using mainly chemical methods. Effective packing specific area and then wetting factor is found to vary with liquid and gas flow rates as well as liquid surface tension. According to Olujic *et al.* (1999), both increased liquid load and low surface tension encourage a more important wetting of the packing surface. Weimer and Schaber (1997) (in Olujic *et al.* (1999)) measured effective surface areas for metal Mellapak 250.Y in the range of 85-95% of the nominal surface area for liquid loads ranging from 15 to 30m^3/m^2h. This result of an interfacial area close to 1 has been recently confirmed by the experiments performed by Tsai *et al.* (2011) on both Mellapak 250 X and Y.

Since we are dealing with Mellapak 250.X (a_g=250 m^2/m^3) in this work, the fractional wetted area f_e is given by the correlation of Brunazzi *et al.* (1997) developed for Mellapack packings. It is written as:

$$f_e = \frac{\sin(\theta)}{a_g} \times \theta_L^{1.5} \times \left(\frac{\rho_L \times g}{3 \times \mu_L \times U_{LS}}\right)^{0.5}$$

where θ refers to the corrugation angle of the packing (channel flow angle from horizontal equal to 60° in the case of Mellapak 250.X) and U_{LS} to the superficial velocity of the liquid defined as follows:

$$U_{LS} = \varepsilon\theta_L \times \left\|\vec{U}_L\right\| .$$

4. Discussion: Comparison between numerical simulations and experimental results

We have performed a 2D axi-symmetric numerical simulations using the numerical code Fluent (version 13) with a pressure based unsteady state solver which appeared to be necessary to avoid numerical divergence. We developed original *user defined functions* for the porous resistances, for the interfacial transfer term and for the dispersive term. The interfacial transfer was implemented through a modification of the drag in a *define exchange properties* function. Resistances and dispersive terms were implemented as source terms using *define properties* functions. The total flow rates are q_L=16m3/m2h for the liquid, and F_S=31.5%F_C=1.16 $Pa^{0.5}$ or F_S=60%F_C=2.21 $Pa^{0.5}$ for the gas. The geometry is adapted to simulate the column where experiments were performed that is described in details in Fourati *et al.* (2012). The domain for the calculations has a radius equal to 0.2m, and a height equal to 0.76m to simulate the part of the real column between liquid injection and the first three layers of structured packing. As shown in Figure 3, we inject the liquid at the top of the column through a central part of radius R_{injL}=12mm. At the inlet, the liquid volume fraction is necessarily set equal to 1, and its velocity set to 1.19m/s to ensure a flow rate equal to the experimental one. Physical gas inlet is at the bottom of the column; however, in order to facilitate counter-current calculations, it appeared that the best way was to fix at the residual part of the top of the column a boundary condition of gas inlet (with a negative velocity along the normal direction of the domain). The velocities of gas are set equal to 1.052m/s and 2m/s respectively for both simulated cases. The bottom of the column is then defined as a pressure outlet where gas and liquid can respectively freely go out of the domain, the gas being also able to re-enter the domain. The domain is also limited by the axis and by a symmetry boundary. The domain of calculation is divided into three parts, the packed bed and an upper and a lower parts of heights 0.1m with no porous resistance that correspond the region empty of packing in the experimental setup and the part of 0.66m high with porous resistances as in the real column upstream and downstream the packed bed respectively. The mesh grid has a size of 15224 nodes with refined grid near the wall and in the central region of the liquid jet. In the radial direction, cell mean size is 0.5 mm in the liquid injection zone and 3 mm elsewhere with bell shaped

sequence. In the axial direction, cell size is set to 5 mm. Second order upwind discretization schemes were used and the time step was about 10^{-4} s in order to ensure numerical convergence.

The simulated cases are described in table 1. We have performed a simulation (case a) without any dispersion term and three others denoted cases b to d with the dispersion term $\vec{F}_{disp,k}$ proposed by Lappalainen *et al.* (2009, 2011). In every case we took the spreading factor D_r=3.7mm as measured in the experiments.

In cases a, b and d, the fractional wetted area was taken equal to 1 as a first approximation. It is thus assumed that, at the local scale, the packing surface is totally covered by a continuous liquid film. One should notice at this point that the references considered in section 3 and analyzing partial wetting deal with homogeneous flows which is not the case for the present experiments and simulations. In fact, calculation of the superficial liquid velocity based on the injection surface leads to relatively important liquid loads so that we could consider, based on the upper bibliographic results, that total wetting is obtained in the limited region where liquid flows.

However, in order to test sensitivity of results to partial wetting, we performed a simulation (case c) considering variable wetting factor based on correlation proposed by Brunazzi *et al.* (1997).

Figure 4 shows the liquid volume fraction contour maps. From the comparison of the cases without or with a dispersion model, one observes that it is essential to use such a model for dispersion to ensure radial spreading of the liquid. Indeed, case a (without dispersion model) provides a very narrow spatial distribution of liquid with an important overconcentration of liquid at its border that could be the memory of the liquid impact on the porous zone. On the contrary, when a model for dispersion is used (case b), both the liquid saturation (Figure 4) and the liquid velocity (Figure 5) spread in the radial direction. The liquid decelerates in the porous medium due to shear stresses at the walls and to interfacial shear stress applied by the countercurrent gas. The pressure distribution is not very sensitive to the distribution of liquid. Figure 6 shows a dominant axial evolution of the pressure as if the liquid inlet conditions were homogeneous. This has already been observed in the experiments were pressure drop was similar for homogeneous injection or central injection of liquid. It may be

explained by the fact that liquid films remain very thin in our flow conditions. The overall predicted pressure gradients ($\Delta P/\Delta z$ = 59.5 Pa/m for F_S=1.16 $Pa^{0.5}$ and $\Delta P/\Delta z$ =114 Pa/m for F_S=2.21 $Pa^{0.5}$) are in good agreement with the ones measured in the experimental set-up (45 and 107 Pa/m in Fourati *et al.* (2012)). This was expected as the model of porous resistance that we took proved to be representative for Mellapak 250.X (Iliuta *et al.*, 2004).

In the non porous zone in the lower part of the simulated column, boundary conditions influence liquid velocity as well as static pressure distributions. Their impact on gas velocity will be discussed further.

On Figure 7 we have reported the radial liquid saturation profiles obtained from gamma-ray tomography at three axial positions of measurement z_1, z_2 and z_3 (Fourati *et al.*, 2012), and the numerical results at the same positions. The experimental values were measured at a different gas flow rate (F_S=0.74 $Pa^{0.5}$) but the comparison is meaningful because the liquid saturation is not sensitive to the gas flow rate in the explored range as observed in the experiments. The agreement between numerical predictions and experimental values is not perfect, but our numerical model predicts the maximum values of the liquid saturation at the three positions, and the liquid jet widens, even if not enough. To test if the fractional wetted area could participate for a part to the radial distribution of liquid, we included the model for f_e in case c. Figure 7.a shows that the wetting model does not govern the radial spreading of the liquid as there is no drastic changes between the spatial distribution of liquid predicted in case b and case c. The liquid distribution predicted by numerical simulations for low and moderate gas flow rates (cases b and d) appears not to vary significantly (Figure 7). This has been also observed through radial experimental profiles of liquid volume fractions reported in Figure 7.

Figure 8 provides radial profiles of the velocities in the liquid and the gas phases at different longitudinal positions. In the liquid phase (Figure 8.b), the axial velocity is far larger than this in the radial direction. The liquid jet main direction is the axial one with momentum diffusion in the radial one. This momentum diffusion is linked to dispersion source term in the momentum balance described in section 3. That does not occur in case a, where no dispersion term is added.

Moreover, gas is also flowing in axial direction mainly (Figure 8.a). In the present simulations, the radial profiles of gas velocity are quite complex. Gas velocity contours in the vicinity of the lower boundary of the column show important accelerations that may be related to the boundary condition at this location and to the inlet of the porous zone (Figure 9). Boundary conditions associated to counter-current gas-liquid flows are complex to handle but these proposed in this work still give representative results: the saturation and the velocity of the liquid phase as well as the pressure show reasonable distributions even if the gas velocity prediction could be improved.

The discrepancy between the radial profiles of θ_L predicted by numerics and the more diffusive profiles obtained in the experiments may come from several effects. We have checked that the numerical results are not sensitive to the mesh grid in the present numerical conditions. The knowledge of an exact value of the spreading factor S may also be crucial for numerical prediction. Concerning this point the experimental method providing the value of S should be precisely discussed and tested. In fact, using the experimental correlation $\theta_L = kq_L^{0.4}$ (Eq. (6) in Fourati *et al.*, (2012)) in order to transform measurements of θ_L into estimations of q_L can introduce artificial distorsion of our estimation of the real spatial distribution of q_L. Approximations or uncertainties in the determination of S may thus appear. But we have checked that our numerical results verify with a satisfactory precision at any local position $\theta_L = kq_L^{0.4}$. Also, there could be differences between the effective numerical transverse momentum balance and the simplified one given in Eq. (11) that is necessary to identify D_r and S. The analysis of the momentum balance will be performed rapidely. At first we have to check the effect of numerical clipping. In fact, we have to deal with strongly non linear terms relatively to θ_k in the modeled porous resistance of the liquid and in the interfacial momentum transfer. We have therefore limited the values of $\vec{S}_{porous,L}$ and $\vec{R}_{IG}$ for asymptotic low values of θ_L and θ_G in the numerical simulations. We have also used clipping in cases a and b (where $f_e = 1$) to ensure that $\vec{S}_{porous,G}$ does not disappear as suggested by the multiplying factor $(1 - f_e)$ in Eq. (7) and applies in cells where gas is alone.

5. Conclusion and perspectives

An Eulerian two-fluid model to predict gas-liquid flows in packed columns has been developed. This model gives a local description of the two-phase flow using volume-averaged quantities. The models of the momentum exchanges at the walls and at the interface between the liquid and the gas are based on the proposal of Iliuta and Larachi (2004). The modeling of liquid dispersion was an important goal of the present study. The model of Lappalainen *et al.* (2009) has been implemented and tested. The comparison of the numerical predictions with recent experimental results obtained in counter-current flow is promising. The difference between experiments and numerics could originate from the selected model of mechanical dispersion. In the absence of firm theoretical basis it is difficult to evaluate the most representative model from Liu and Long (2000) or from Lappalainen *et al* (2009). Testing a model derived from Liu and Long (2000) will be the next step of our study.

Notations

Latin letters

a_g packing external surface area per unit volume of packed bed, m^2/m^3

A_k viscous permeability for phase k

C_k coefficient of the inertial isotropic resistance

$\overline{\overline{C}}_k$ inertial resistance tensor for phase k

D_r liquid spread factor, m

$\overline{\overline{D}}_k$ viscous resistance tensor for phase k

e liquid film thickness, m

E_1, E_2 Ergun coefficients

f_e fractional wetted area

F_S gas capacity factor, $Pa^{0.5}$

F_C gas capacity factor at flooding conditions, $Pa^{0.5}$

$\vec{F}_{disp,k}$ dispersive term in the momentum equation of phase k

g gravity acceleration, ms^{-2}

H interface curvature, m^{-1}

h_k width of phase k in a slit, m

K_{IG} coefficient in the law of $\vec{R}_{IG}$

K_{kS} coefficient in the law of $\vec{S}_{porous,k}$

$\overline{\overline{K}}_L$, $\overline{\overline{K}}_{IG^*}$ dispersion tensors

l_k size of phase k at the pore scale, m

P Pressure, Pa

q_L liquid load, $m^3m^{-2}h^{-1}$

r radial component in a cylindrical coordinate system

$\vec{R}_{Ik}$ average momentum transfer term at the interface for phase k

$\vec{S}_{porous,k}$ average momentum transfer at the wall for phase k

S spread factor (m)

$\overline{\overline{S}}$ spreading tensor

U_{GS} gas superficial velocity, ms^{-1}

U_{LS} liquid superficial velocity, ms^{-1}

$\vec{U}_k$ intrinsic volume-average velocity of phase k, ms-1

$\vec{U}_{D,k}$ drift velocity of phase k

z axial component in a cylindrical coordinate system

Greek letters

α_k volume fraction of phase k

$\Delta P/\Delta z$ pressure drop, $Pa.m^{-1}$

ε packing void fraction, porosity, dimensionless

θ angle with the horizontal direction or azimuthal component in a cylindrical coordinate system

θ_k saturation of phase k

μ_k dynamic viscosity of phase k, Pas^{-1}

ρ_k density of phase k, kgm^{-3}

σ surface tension, Nm^{-1}

τ_k tortuosity of phase k

$\overline{\overline{\tau_k}}$ averaged viscous stress tensor in phase k

Subscript

C capillary

G gas phase

L liquid phase

s solid

w wall

References

Alix, P and L. Raynal, 2008. Liquid distribution and liquid hold-up in modern high capacity packings. *Chem. Eng. Res. and Design*, 86,6A, pp 585-591.

Alix, P., L. Raynal, F. Abbe, M. Meyer, M. Prevost and D. Rouzineau. 2011. Mass transfer and hydrodynamic characteristics of new carbon carbon packing : Application to CO2 post-combustion capture. *Chem. Eng. Res. and Design*, 89, 1658-1668.

Attou A., Boyer C., Ferschneider G., Modelling of the hydrodynamics of the cocurrent gas-liquid trickle flow through a trickle-bed reactor, Chemical Engineering Science 54 (1999) pp. 785-802.

Attou A., Ferschneider G., A two-fluid hydrodynamic model for the transition between trickle an pulse flow in a cocurrent gas-liquid packed-bed reactor, Chemical Engineering Science 55 (2000) pp. 491-511.

Brenner H., Dispersion resulting from flow through spatially periodic porous media, Phil. Trans. Royal Soc., series A, vol. 297, n° 1430, pp. 81-133, 1980.

Boyer C., Koudil A., Chen P., Dudukovic, Study of liquid spreading from a point source in a trickle bed via gamma-ray tomography and CFD simulation, Chemical Engineering Science, vol. 60, 2005, pp. 6279-6288.

Brunazzi E., Paglianti A., Mechanistic Pressure Drop Model for Columns Containing Structured Packings, AIChE Journal, vol. 43, n°2, pp. 317-327, 1997

Carbonell R. G., Whitaker S., Dispersion in pulsed systems – II Theoretical developments for passive dispersion in porous media, Chemical Engineering Science, vol. 38, n° 11, pp. 1795-1802, 1983.

Eidsath A., Carbbonell R. G., Whitaker S., Herrmann L. R., Dispersion in pulsed systems – II Comparison between theory and experiments for packed beds, Chemical Engineering Science, vol. 38, n° 11, pp. 1803-1816, 1983.

Ergun S., Fluid flow through packed columns, Chemical Engineering Progtress, vol. 48, n°2, pp. 89-94, 1952

Fourati M., Roig V., Raynal L., Experimental study of liquid spreading in structured packings, Chemical Engineering Science, vol. 80, pp. 1-15, 2012.

Grosser K., Carbonell R. G., Sundaresan S., Onset of pulsing in two-phase cocurrent downflow through a packed bed, AIChE Journal, vol. 34, n° 11, pp. 1850-1860, 1988.

Holub R. A., Dudukovic M. P., Ramachandran P. A., Pressure drop, Liquid holdup and flow regime transition in trickle flow, AIChE Journal, vol. 39, n° 2, pp. 302-321, 1993.

IEA Ed., available at http://www.iea.org/papers/2009/CCS_Roadmap.pdf .

Iliuta I., Petre C. F., Larachi F., Hydrodynamic continuum model for two-phase flow structured-packing-containing columns, Chemical Engineering Science, vol. 59, pp. 879 – 888, 2004.

Iliuta I., Larachi F., Modelling the Hydrodynamics of Gas-Liquid Packed Beds via Slit Models: A Review, International Journal of Chemical Reactor Engineering, vol. 3, Review 4., 2005

Iliuta R. A., Dudukovic M. P., Ramachandran P. A., Pressure drop, Liquid holdup and flow regime transition in trickle flow, AIChE Journal, vol. 39, n° 2, pp. 302-321, 1993.

Iliuta R. A., Larachi F., Al-Dahhan M. H., Double-slit model for partially wetted trickle flow hydrodynamics, AIChE Journal, vol. 46, n° 3, pp. 597-609, 2000.

Jiang Y., Khadilkar M. R., Al-Dahhan M. H., Dudukovic M. P., CFD of Multiphase Flow in Packed-bed Reactors: I. *k*-Fluid Modeling Issues, AIChE Journal, vol. 48, n° 4, pp. 701-715, 2002.

Lappalainen K., Gorshkova E., Manninen M., Alopaeus V., Characteristics of liquid and tracer dispersion in trickle-bed reactors: effect on CFD modelling and experimental analyses, Computers and Chemical Engineering, vol. 35, pp. 41-49, 2011.

Lappalainen K., Manninen M., Alopaeus V., Aittamaa J., Dodds J., An analytical model for capillary pressure-saturation relation for gas-liquid system in a packed-bed of spherical particles, Transport in Porous Media, vol. 77, pp. 17-40, 2009-b.

Lappalainen K., Manninen M., Alopaeus V., CFD modelling of radial spreading of flow in trickle-bed reactors due to mechanical and capillary dispersion, Chemical Engineering Science, vol. 64, pp. 207-218, 2009.

Liu S., A continuum approach to multiphase flows in porous media, Journal of Porous Media, 2(3), pp. 295-308, 1999.

Liu S., J. Long, Gas-liquid countercurrent flows through packed towers, Journal of Porous Media, 3(2), pp. 99-113, 2000.

Macdonald I. F., El-Sayed M. S., Mow K. and Dullien F. A. L., Flow through Porous Media: the Ergun Equation Revisited, Ind. Eng. Chem. Fundam., Vol. 18, No. 3, pp. 199-208,1979

Mewes D, Loser T., Millies M., Modelling of two-phase flow in packings and monoliths , vol. 54, pp. 4729-4747, 1999, Chemical Engineering Science

Mewes D., Loser T., Millies M., Modelling of two-phase flow in packings and monoliths, Chemical Engineering Science, vol. 54, pp. 4729-4747, 1999.

Olujic Z, Kamerbeek A. B., de Graauw J., A corrugation geometry based model for efficiency of structured distillation packing, Chemical Engineering and Processing, vol.38, pp. 683–695, 1999

Quintard M., Whitaker S., Transport in ordered and disordered porous media: volume-averaged equations, closure problems and comparison with experiments, Chemical Engineering Science, vol. 48, n° 14, pp. 2537-2564.

Raynal L. and Royon-Lebeaud A., A multi-scale approach for CFD calculations of gas–liquid flow within large size column equipped with structured packing, Chemical Engineering Science, vol. 62, pp. 7196-7204, 2007.

Raynal, L., PA. Bouillon, A. Gomez and P. Broutin, From MEA to demixing solvents and future steps, a roadmap for lowering the cost of post-combustion carbon capture. *Chem. Eng. J.* 171, pp. 742-752, 2011.

Sulzer - reducing the energy penalty for post-combustion CO2 capture, A. Menon, M. Duss, Carbon Capture J. 23, 2-5, (2011).

Tsai R.E., Seibert A.F., Eldridge R.B. and Rochelle G.T., 2011, A dimensionless model for predicting the mass-transfer area of structured packing, AIChE J. 57 (5), 1173-1184.

Vafai K., Handbook of porous media (Chapter by Liu S. and Masliyah J. H.: Dispersion in porous media), CRC Press, Taylor and Francis Group, 2005.

Valdes-Parada F. J., J. A. Ochoa-Tapia, J. Alvarez-Ramirez, Validity of the permeability Carman-Kozeny equation: A volume averaging approach, Physica A, vol. 388, pp. 789-798, 2009

Whitaker S., Flows in porous media II: The governing equations for immiscible, two-phase flow, Transport in Porous Media, 1, pp. 105-125, 1986.

Whitaker S., The Method of Volume Averaging, Kluwer Academic Publishers, Dordrecht, 1999

Whitaker S., The transport equations for multi-phase systems, Chemical Engineering Science, vol. 28, pp. 139-147, 1973

Tables

Table 1: simulated cases

Cases	Wetting factor f_e	Dispersion model	$q_L(m^3/m^2h)$	F_S ($Pa^{0.5}$)
a	1	No	16	1.16
b	1	Yes	16	1.16
c	Brunazzi et al. (1997)	Yes	16	1.16
d	1	yes	16	2.21

Figure captions

Figure 1: Liquid hold-up maps for 2 runs with air and water in Mellapak 250.X, *qL=16* m3/m2h, a/ case A: *FS=0.74Pa0.5,* b/ case B: *FS=2.21Pa0.5. (Positions* from left to right: z1, z2, z3 & z4).

Figure 2: Scheme of the two-phase flow in a slit

Figure 3: Mesh and boundary conditions. (The porous zone is in between both blue dashed lines)

Figure 4: Spatial distribution of liquid volume saturation θ_L . (qL=16 m3/m2h, FS=31.5%FC), left: case a (without dispersion model), right: case b (with dispersion model).

Figure 5: Contours of liquid velocity magnitude (in m/s). (qL=16 m3/m2h, FS=31.5%FC), case b.

Figure 6: Pressure field (Pa). (qL=16 m3/m2h, FS=31.5%FC), case b.

Figure 7: Radial profiles of liquid saturation $\theta_{L\,\mathrm{from}}$ simulations and experiences for qL=16m3/m2h. FS=0.74 Pa0.5 for the experiments and: a/ *FS*= 1.16Pa0.5 (cases a and b of Table 1), b/ *FS=2.21Pa0.5,* (case d of Table 1).

Figure 8: Radial profiles of a) gas and b) liquid velocity for simulations at qL=16m3/m2h and *FS=31.5%FC*

Figure 9: Contours of gas velocity magnitude (m/s). (qL=16 m3/m2h, FS=31.5%FC)

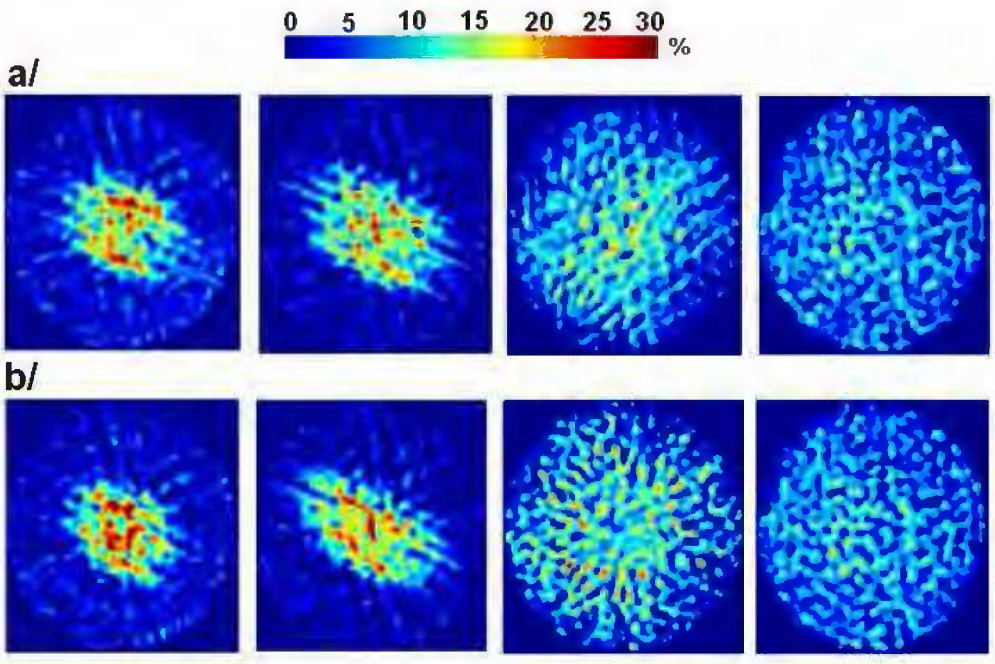

Figure 1: Liquid hold-up maps for 2 runs with air and water in Mellapak 250.X, q_L=16 m^3/m^2h, a/ case A: F_S=0.74$Pa^{0.5}$, b/ case B: F_S=2.21$Pa^{0.5}$. (Positions from left to right: z_1, z_2, z_3 & z_4).

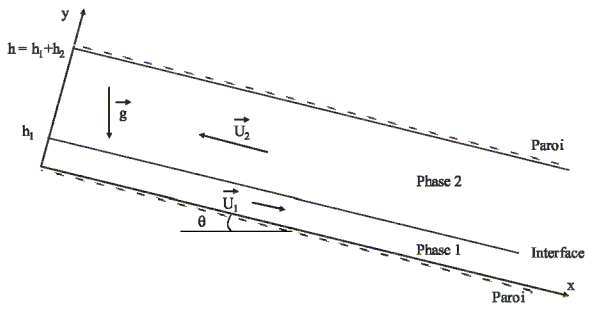

Figure 2: Scheme of the two-phase flow in a slit

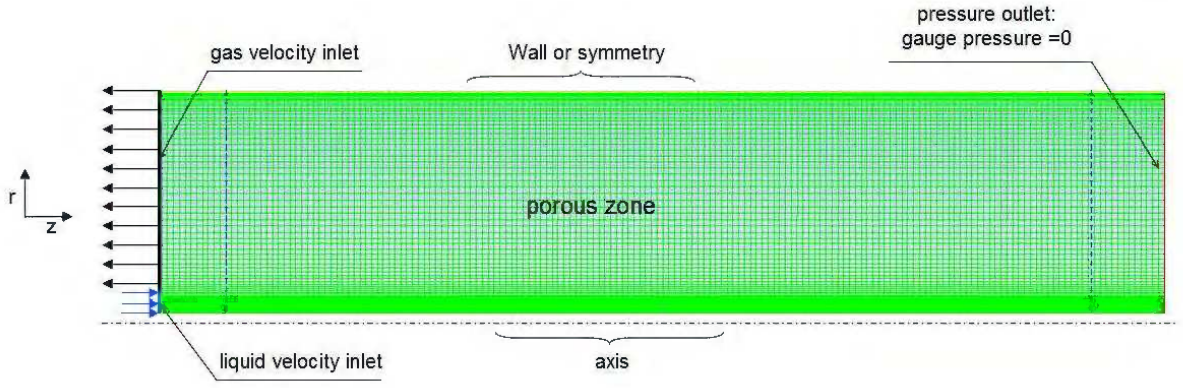

Figure 3: Mesh and boundary conditions. (The porous zone is in between both blue dashed lines)

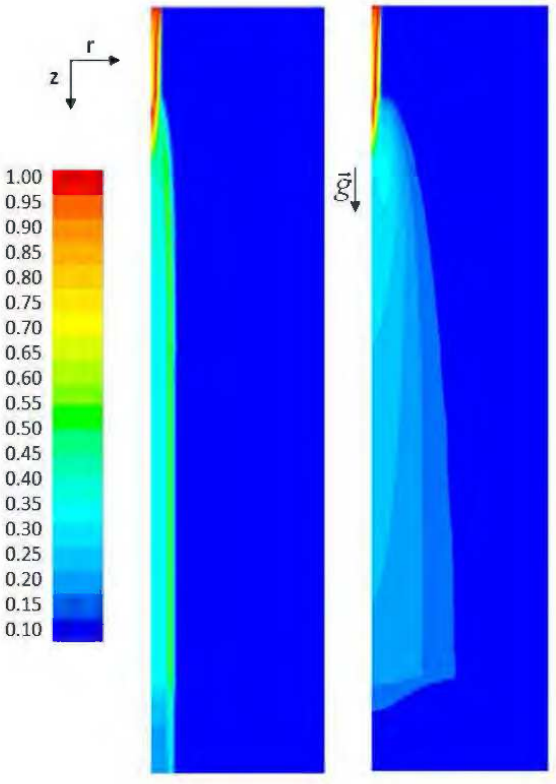

Figure 4: Spatial distribution of liquid volume saturation θ_L . (q_L=16 m3/m2h, F_S=31.5%F_C), left: case a (without dispersion model), right: case b (with dispersion model).

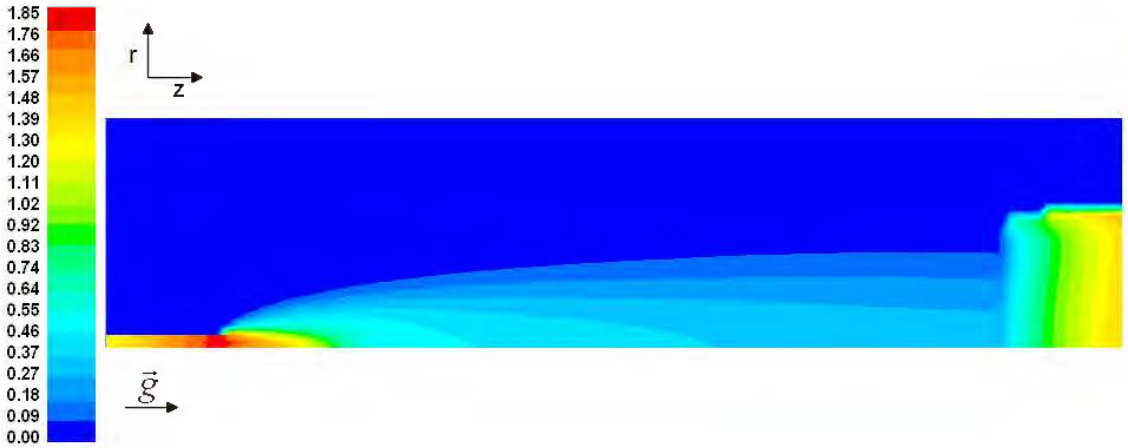

Figure 5: Contours of liquid velocity magnitude (in m/s). (q_L=16 m3/m2h, F_S=31.5%F_C), case b.

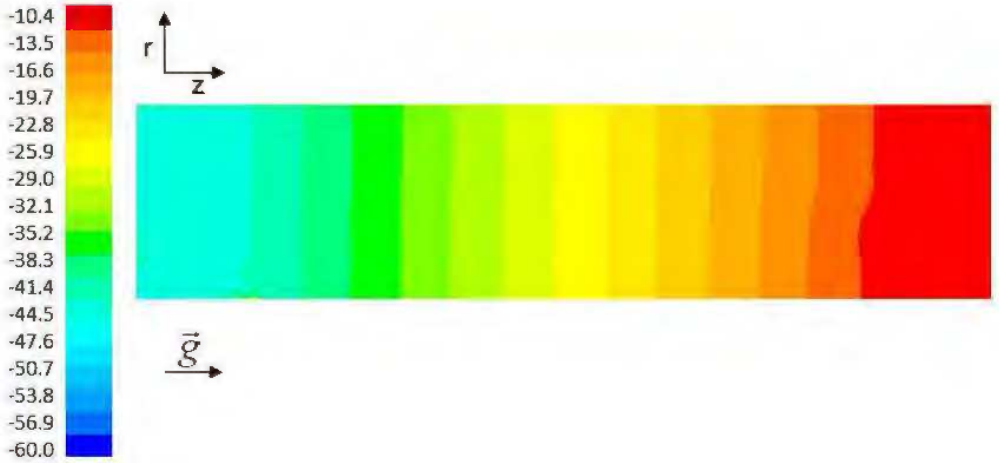

Figure 6: Pressure field (Pa). (q_L=16 m3/m2h, F_S=31.5%F_C), case b.

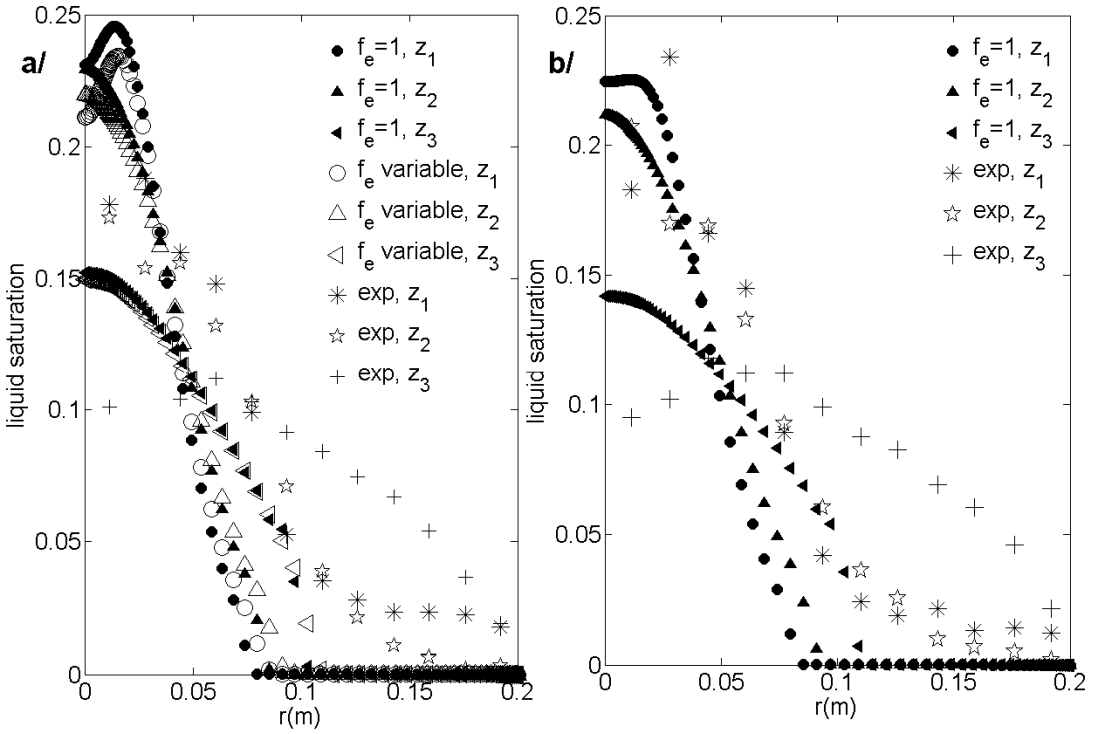

Figure 7: Radial profiles of liquid saturation θ_L from simulations and experiences for q_L=16m3/m2h. F_S=0.74 $Pa^{0.5}$ for the experiments and: a/ F_S= 1.16$Pa^{0.5}$ (cases a and b of Table 1), b/ F_S=2.21$Pa^{0.5}$, (case d of Table 1).

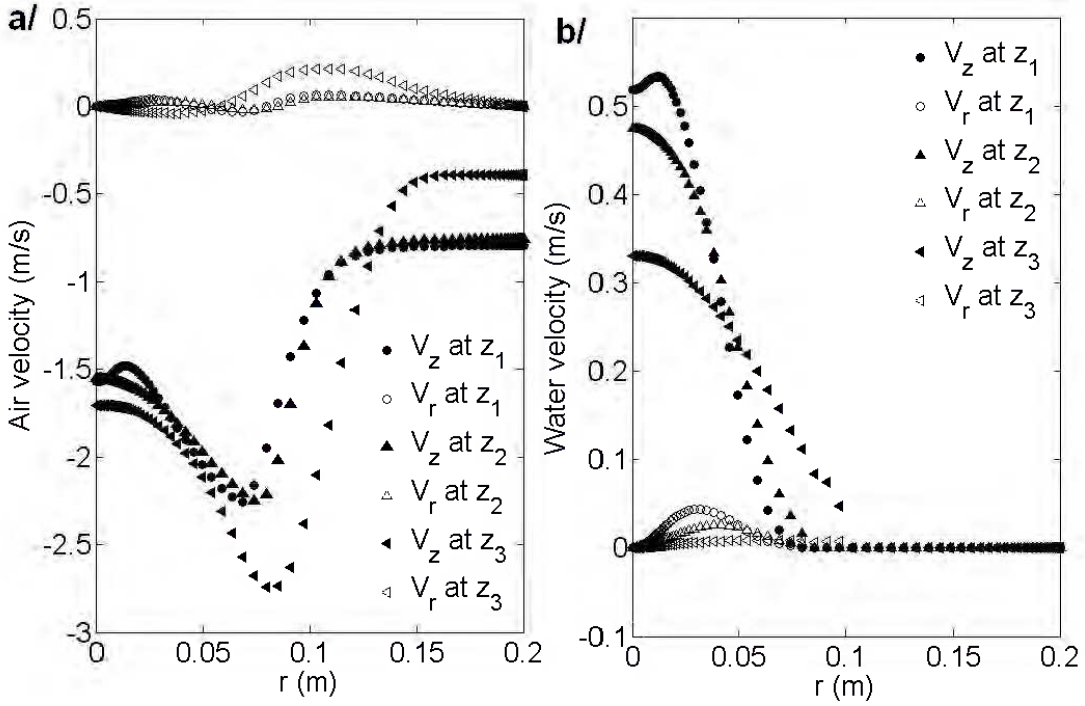

Figure 8: Radial profiles of a) gas and b) liquid velocity for simulations at q_L=16m^3/m^{2}h and F_S=31.5%F_C

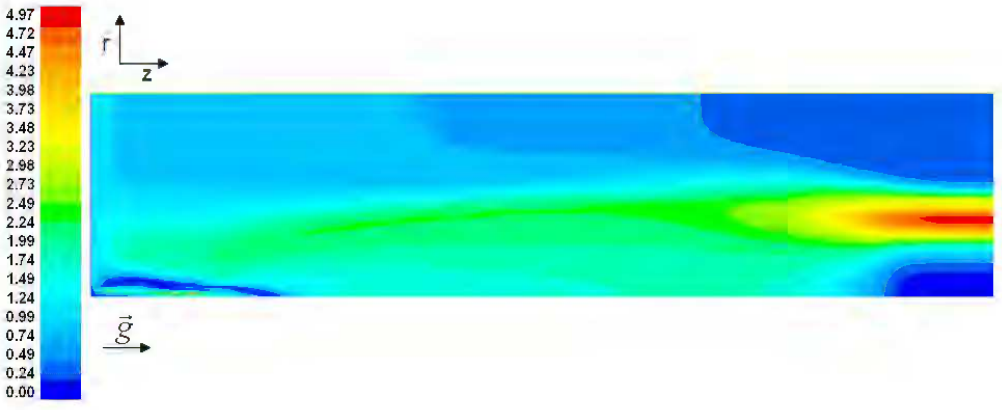

Figure 9: Contours of gas velocity magnitude (m/s). (q_L=16 m3/m^{2}h, F_S=31.5%F_C)